



Chemical reaction mechanisms between Y_2O_3 stabilized ZrO_2 and Gd doped CeO_2 with PH_3 in coal syngas



Gang Chen ^{a,*}, Haruo Kishimoto ^a, Katsuhiko Yamaji ^a, Koji Kuramoto ^a, Mingyang Gong ^b, Xingbo Liu ^b, Gregory Hackett ^c, Kirk Gerdes ^c, Teruhisa Horita ^a

^a National Institute of Advanced Industrial Science and Technology, Tsukuba, Japan

^b Dept. of Mechanical & Aerospace Engineering, West Virginia University, Morgantown, USA

^c National Energy Technology Laboratory, Morgantown, USA

HIGHLIGHTS

- Stabilities of YSZ, GDC in CSG with different concentrations of PH_3 were investigated.
- Significant reactions between YSZ and GDC with 10 ppm PH_3 in CSG were confirmed.
- Reaction mechanisms between YSZ and GDC with PH_3 were clarified.
- YSZ shows better phosphorus resistance than GDC in CSG with low concentration of PH_3 .

ARTICLE INFO

Article history:

Received 17 March 2014

Received in revised form

20 May 2014

Accepted 23 June 2014

Available online 7 July 2014

Keywords:

Integrated coal gasification combined cycle
Solid oxide fuel cell
 PH_3
 Y_2O_3 stabilized ZrO_2
Gd doped CeO_2
Coal syngas

ABSTRACT

To clarify the chemical stability of the key materials exposed to coal syngas (CSG) containing PH_3 contaminant atmosphere, exposure tests of Y_2O_3 8 mol.% stabilized ZrO_2 (YSZ) and Gd doped CeO_2 (GDC) are carried out in simulated CSG with different concentrations of PH_3 . Significant reaction between YSZ and 10 ppm PH_3 in CSG atmosphere is confirmed, and no obvious reaction is detected on the surface of YSZ after exposed in CSG with 1 ppm PH_3 . YPO_4 , $\text{Zr}_{2.25}(\text{PO}_4)_3$ and monoclinic Y partial stabilized ZrO_2 (m-PSZ) are identified on the YSZ pellet surface after exposed in CSG with 10 ppm PH_3 . GDC reacted with PH_3 even at 1 ppm concentration. A $(\text{Ce}_{0.9}\text{Gd}_{0.1})\text{PO}_4$ layer is formed on the surface of GDC pellet after exposure in CSG with 10 ppm PH_3 . Possible reaction mechanisms between YSZ and GDC with PH_3 in CSG are clarified. Compared with GDC, YSZ exhibits sufficient phosphorus resistance for devices directly exposed to a coal syngas atmosphere containing low concentration of PH_3 .

© 2014 Elsevier B.V. All rights reserved.

1. Introduction

Coal-fired power generation emits significant CO_2 and features a relatively low electrical conversion efficiency [1,2]. To reduce CO_2 and pollutant emissions and improve the thermal efficiency of coal, integrated coal gasification combined cycle (IGCC) and integrated coal gasification fuel-cell combined cycle (IGFC) systems have been developed [1–4]. An IGFC with a solid oxide fuel cell (SOFC) can directly generate and utilize coal syngas (CSG) with a high power generation efficiency [1,2]. Reliability and performance of the materials in each subsystem are the key factors for the practical IGFC applications.

* Corresponding author. Tel.: +81 (0) 29 861 4542; fax: +81 (0) 29 861 4540.

E-mail addresses: chen-gang@aist.go.jp, chengang@smm.neu.edu.cn (G. Chen).

CSG is a gas mixture containing H_2 , CO , CO_2 , H_2O , CH_4 , N_2 with impurities typically including H_2S , PH_3 , HCl , and AsH_3 [5]. At present, no accurate data are available that describe the nature of phosphorous compounds in the coal syngas. However, thermodynamic calculations indicate that P may exist as $(\text{P}_2\text{O}_5)_2$ (g) and PH_3 (g) in the gas cleanup system [5,6]. Hackett et al. detected very small amounts of phosphorus by ToF-SIMS and XPS in Ni-YSZ SOFC anode after cells were tested in on-line gasified coal syngas [7]. To date, no cleanup techniques can completely remove the impurities without consuming part of the syngas thermal energy [5,6]. Thus, materials with good impurities tolerance are needed for construction of the IGFC subsystems, particularly the coal gasifier, SOFC, and Gas Turbine (GT) that are directly exposed to CSG.

Stabilized zirconia doped with Y_2O_3 or Sc_2O_3 could be used in a gasifier, SOFC and GT, owing to their outstanding robustness [8–13]. In the gasifier, YSZ is utilized as a sensor material to detect

oxygen and carbon monoxide [8,9]. YSZ is also an excellent thermal barrier coating (TBC) material in gas turbines and jet engines to reduce the surface temperature of metallic components [10,11]. In SOFC, Yttrium or Scandium stabilized zirconia (YSZ and ScSZ) are commonly used electrolyte materials [12,13]. In addition to stabilized zirconia, the commonly used SOFC electrolyte material contains Gd- or Sm-doped ceria (SDC or GDC) and perovskite electrolyte material (strontium/magnesium doped lanthanum gallate, LSGM) [12,13].

The impurities in coal syngas with high chemical reactivity could interact with the component material of IGFC subsystem and result in serious performance degradation, particularly in SOFC [6,14–19]. Many reports have been published describing performance degradation of SOFC caused by CSG impurity poisoning [15–23]. Indeed, PH₃ contained in CSG exhibits very high reactivity with SOFC anode material even at 0.5 ppm level [15–19]. The fuel on the anode can directly flow to the electrolyte surface, thus the chemical reactivity between electrolyte materials and phosphorus in CSG has priority in the study of CSG fuelled SOFC.

Phosphorus poisoning of Ni-electrolyte cermet anodes has been reported by several authors [15–19]. Chemical reaction between Ni and phosphorus-containing fuels resulted in irreversible degradation in cell performance [16,19]. Kishimoto et al. constructed the chemical potential diagrams of Ni–P–O–H system through thermodynamic calculation to investigate the chemical stability of Ni anode in fuel containing phosphorous compounds [24]. The Ni–P–O chemical potential diagram indicated that Ni phosphide was formed at low oxygen partial pressure and high P partial pressure atmosphere, and the Ni phosphate was formed at high oxygen partial pressure and low P partial pressure atmosphere [24]. At SOFC operating condition, Ni_mP_n forms in fuel with ppb level of phosphorous [18]. Xu et al. found Ni₅P₂ and Ni₁₂P₅ as the dominant composition of Ni_mP_n in fuels with and without H₂O, respectively [16]. To date, anode material with ceramic structure is widely studied to resist phosphorus poisoning [25–27]. Our recent study found that A-site deficient perovskite La-substituted SrTiO₃ (LST) could effectively suppress chemical reaction between LST and 1 ppm PH₃ in CSG better than the stoichiometric perovskite [27].

Published data indicate that cerium phosphate (CePO₄) and zirconium phosphate (ZrP₂O₇) were detected in Ni-GDC and Ni-YSZ anode material after exposure to the PH₃-containing syngas [14–17]. However, the details of reaction mechanisms between GDC and YSZ with PH₃ in CSG are still unclear. In this study, exposure tests were carried out for pellets in CSG with different concentrations of PH₃ to clarify the reaction mechanism between YSZ and GDC with PH₃ in CSG. The chemical reactions occurring on the pellets were identified by XRD and SEM-EDS system. Possible reaction mechanisms were proposed according to characterization results.

2. Experimental

Y₂O₃ 8 mol.% stabilized ZrO₂ (YSZ, Tosoh Corporation) and Ce_{0.9}Gd_{0.1}O₂ (GDC, Anan Kasei Co. Ltd.) powders were pressed into pellet form by an isostatic press and sintered at 1400 °C for 5 h in air. Before exposure test, the pellet surface was polished. As-prepared YSZ and GDC discs were then placed into a high-density alumina tube for exposure testing in different CSG composition with different PH₃ concentration. The samples were raised to the testing temperature (900 °C) at a rate of 3 °C min⁻¹ under a nitrogen flow. After the samples were heated overnight, the CSG was supplied to the samples. Two simulated CSG compositions were used in this study (CSG1: 17%H₂, 39%H₂O, 16%CO and 28%CO₂; CSG2: 28%H₂, 28%H₂O, 25%CO and 19%CO₂). The estimated oxygen partial pressures ($p(O_2)$) in the simulated CSG as determined from a

conventional Gibbs Free Energy minimization at 900 °C were 2.52×10^{-16} and 4.79×10^{-17} for CSG1 and CSG2, respectively. After stabilizing the tube temperature with nitrogen gas at 900 °C, simulated CSG with different concentrations of PH₃ (1 ppm and 10 ppm) were introduced into the system. The source gas cylinder was 75 ppm PH₃ with balance H₂. Phosphine was introduced through a secondary “contaminant line”. After the samples were annealed for 100 h, the fuels were stopped and the system was set to cool down at 5 °C min⁻¹ under 100% nitrogen flow. The YSZ pellets were exposed in CSG1 with 1 ppm PH₃ and CSG2 with 10 ppm PH₃, and GDC was exposed in CSG1 with 1 ppm PH₃ and CSG1 with 10 ppm PH₃. The phase and microstructure of pellets before and after exposure testing were examined by X-ray diffraction (XRD) and scanning electron microscope/Energy Dispersive Spectrometer + Wavelength Dispersive Spectrometer system (SEM/EDS + WDS). It should be noted that the test device (including all supply tubing) was purged by nitrogen for 8 h and the temperature was raised to 900 °C. The experiment with 1 ppm PH₃ exposure was carried out after all pipelines were replaced, to prevent cross-contamination from the higher-concentration exposure testing. This experimental protocol ensures that the specimens are exposed to the expected PH₃ concentration.

3. Results and discussion

3.1. Exposure results of YSZ

Exposure of the YSZ to 10 ppm PH₃ generated a multi-layer surface structure composed of stratified Y and Zr phases. Fig. 1 depicts the backscattered electron SEM images of the surface and the cross section of YSZ before and after exposure to different CSG and PH₃ conditions. Comparison of Fig. 1(a) (as-fabricated sample) and Fig. 1(b) (1 ppm PH₃) reveals no obvious change on the YSZ surface indicating that no obvious chemical reaction occurs between YSZ and 1 ppm PH₃ in CSG1 at 900 °C. However, as shown in Fig. 1(c), obvious changes occur on the surface of YSZ after exposure test in CSG2 with 10 ppm PH₃. The initially smooth and dense surface of YSZ became rough after exposure as large particles formed. Fig. 1(d) shows the cross section of the YSZ pellet after exposed in CSG2 with 10 ppm PH₃. Several layers with different colour were formed on the surface of YSZ pellet, indicating that several different phases were generated from reactions between YSZ and 10 ppm PH₃ in CSG2.

Fig. 2 shows the XRD patterns of the surface of YSZ pellets before and after exposure in different conditions. As indicated in Fig. 2(b), no obvious additional peak was observed in XRD pattern of YSZ pellet after exposed in CSG1 with 1 ppm PH₃, which agreed well with the SEM result shown in Fig. 1(b). YPO₄, Zr_{2.25}(PO₄)₃ and monoclinic Y partial stabilized ZrO₂ (m-PSZ) peaks were observed in Fig. 2(c), which confirmed that significant chemical reactions occurred on the surface of YSZ after exposed in CSG2 with 10 ppm PH₃.

Fig. 3 shows the elemental maps of the cross section of the YSZ pellet after exposure test in CSG2 with 10 ppm PH₃. Here the maps of P, Y and Zr were identified by WDS due to the adjacent peaks of P, Y and Zr in EDS pattern. As indicated in the elemental map shown in Fig. 3, the main constituents of the light grey surface phase are Y and P, and the main constituents of the dark grey phase are Zr and P. Highlighted P can be observed in both layers (light grey layer and dark grey layer). The Y map exhibits a thin Y-enriched layer under the dark grey phase layer. Under the Y enriched layer, a layer exists with insufficient Y and enriched Zr, with limited P also observed.

Table 1 shows the point analyses of the additional phase layers apparent in the SEM cross section image of Fig. 3. The detection area of EDX “point” analysis is actually a circular region approximately 1 μm in diameter. Therefore, the data in Table 1 are used as a

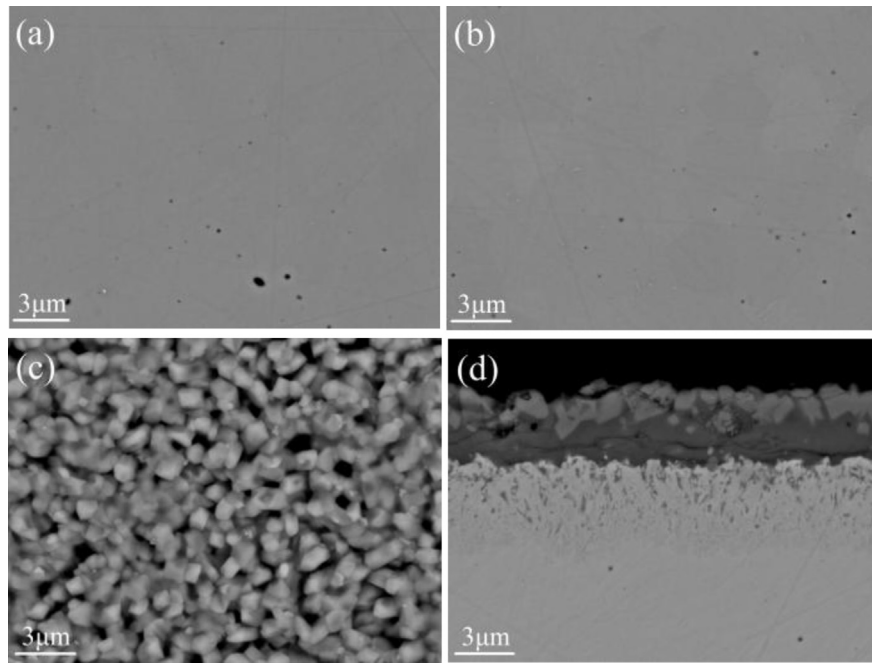


Fig. 1. SEM images of the surface and the cross section of YSZ pellets before and after exposure in different conditions, (a) surface of fresh pellet, (b) surface after exposure to CSG1 with 1 ppm PH₃, (c) surface after exposure to CSG2 with 10 ppm PH₃, (d) cross section after exposure to CSG2 with 10 ppm PH₃.

qualitative reference to support the XRD and SEM/WDS results. According to atomic ratio of each element and the XRD result shown in Fig. 2(c), the main phase of the light grey layer (spectrum 1,2 and 3) is YPO₄, and the dark grey phase is Zr_{2.25}(PO₄)₃ (spectrum 4, 5 and 6). The main phases around spectrum 7, 8 and 9 could be m-PSZ and little YPO₄. The YPO₄ phase under the dark grey layer is scattered near the Zr_{2.25}(PO₄)₃ layer, under which is the m-PSZ layer. Under the m-PSZ layer is the YSZ without reaction. The thickness of the reaction layer (including YPO₄, Zr_{2.25}(PO₄)₃ and m-PSZ layers) in the YSZ pellet shown in SEM image of Fig. 3 is about 10 μm.

3.2. Exposure results of GDC

Fig. 4 shows the backscattered electron SEM images of the GDC pellet surface before and after exposure in CSG1 with different PH₃

concentrations at 900 °C for 100 h. As indicated in Fig. 4 (a), (b) and (c), obvious structural and morphological changes were observed on the surface of GDC pellets after exposure test in CSG1 with 1 ppm and 10 ppm PH₃. The appearance of the GDC surface depended on the PH₃ exposure condition. Compared with the smooth surface of the fresh GDC pellet, the GDC pellet surface became rough after exposure in CSG1 with 1 ppm PH₃ (as shown in Fig. 4 (b)), but the GDC pellet surface remained smooth after exposure in CSG1 with 10 ppm PH₃ (as shown in Fig. 4 (c)). Big particles and clear grain boundaries between each particle were observed.

The backscattered electron SEM image shown in Fig. 4(d) indicates that an additional 3 μm thick phase layer (different extrinsic feature compared with GDC phase) was formed on the surface of GDC pellet after exposed in CSG1 with 10 ppm PH₃. Moreover, compared with the GDC pellet, the mechanical strength of the additional phase layer is very low, and the connectivity between the generated phase layer and GDC is also poor. Thus, the additional phase layer formed on the GDC surface can be easily crushed and peeled.

Fig. 5 shows the XRD patterns of the GDC pellet surface before and after exposure in CSG1. Additional phase peaks were observed in each sample after exposure in CSG1 with 1 ppm PH₃ and in CSG1 with 10 ppm PH₃, respectively. According to the intensities of additional phase depicted in Fig. 5 (b) and (c), more significant reactions occurred on the surface of GDC exposed in CSG1 with 10 ppm PH₃. The additional phase peaks in XRD pattern essentially correspond with monazite Ce(PO₄) [28]. No obvious peak in the pattern matched any known Gd phosphate.

Fig. 6 depicts the elemental maps of the GDC pellet cross section after exposure testing in CSG1 with 10 ppm PH₃. From Fig. 6, the main constituents of the additionally formed surface phase are Ce, Gd and P. Table 2 shows the lattice parameters of the additional phase shown in the XRD pattern of Fig. 5(c), which are monazite CePO₄ and GdPO₄ reported in Refs. [28–30]. The structure of monazite is generally described as the nine-fold coordination of the metallic cation interpenetrated by a tetrahedron constructed from 4 oxygen atoms belonging to two bidentate tetrahedrons [30]. As indicated in the XRD pattern of Fig. 5(c), the peak positions of the

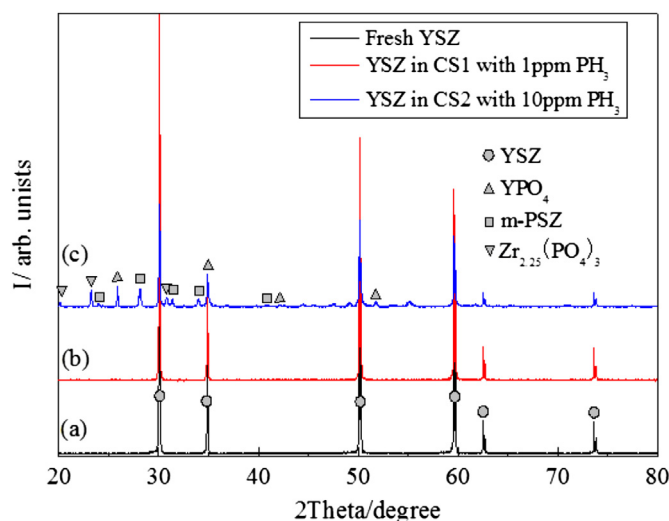


Fig. 2. XRD patterns of the surface of YSZ pellets before and after exposure to different conditions, (a) fresh pellet, (b) in CSG1 with 1 ppm PH₃, (c) in CSG2 with 10 ppm PH₃.

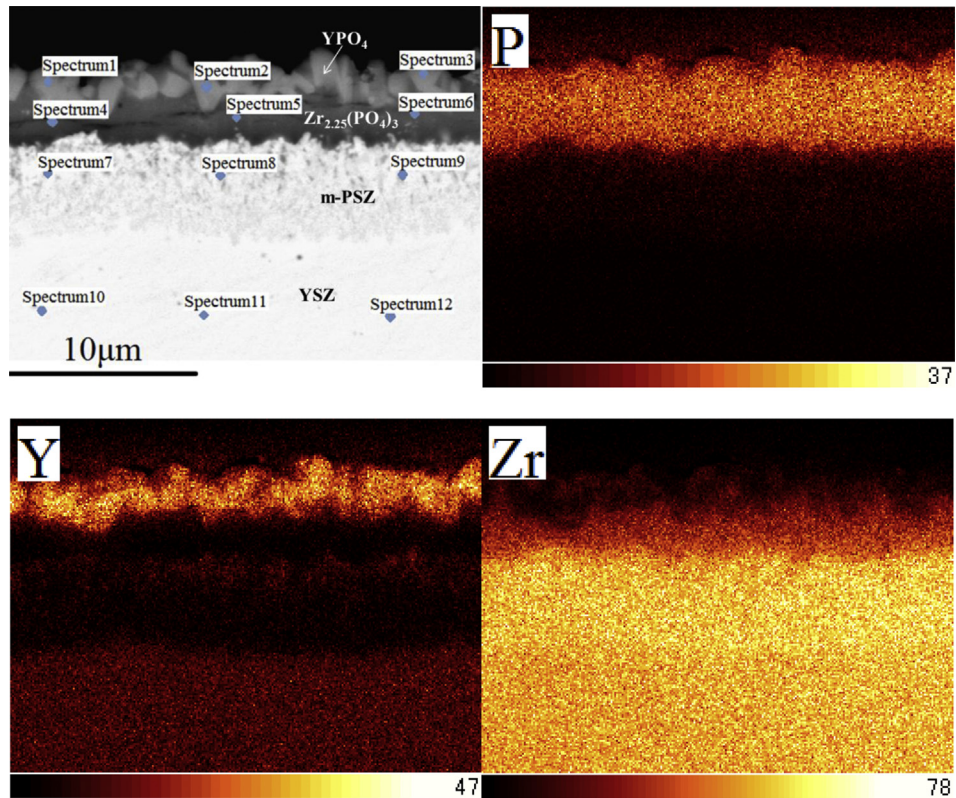


Fig. 3. Elemental maps of the cross section of YSZ pellet after exposure testing in CSG2 with 10 ppm PH₃.

Table 1

Point analysis of the additional phase layer indicated in cross section SEM image of Fig. 3.

Spectrum no.	Elemental (at.%)				Possible phase compositions
	O	Y	Zr	P	
Spectrum 1	67.2	13.5	2.0	17.2	
Spectrum 2	67.4	13.9	1.5	17.2	
Spectrum 3	65.9	15.0	1.3	17.8	
Spectrum 4	69.8	0	13.5	17.6	
Spectrum 5	70.7	0	13.9	16.6	
Spectrum 6	71.5	0	13.4	16.0	
Spectrum 7	69.0	1.2	29.5	0.3	
Spectrum 8	68.5	3.0	26.3	2.2	m-PSZ + YPO ₄
Spectrum 9	67.3	3.3	26.6	2.8	
Spectrum 10	67.3	4.9	29.9	0	
Spectrum 11	67.7	4.5	29.0	0	
Spectrum 12	67.0	4.7	29.5	0	YSZ

additional phase principally agree with those of CePO₄. Thus, the lattice parameters of the additional phase were calculated with the indices of CePO₄. The atomic radius of Ce and Gd were 1.85 Å and 1.8 Å, respectively [30]. The average bond distances of Ce–O (2.556 Å) in the ninefold coordination geometry of CePO₄ were smaller than those of Gd–O (2.469 Å) in the ninefold coordination geometry of GdPO₄. The bond distances of P–O in tetrahedrons of CePO₄ and GdPO₄ were 1.538 Å and 1.53 Å, respectively [28,29]. From Table 2, all of the parameters (a, b, c and β) of additional phase were slightly diminished compared to CePO₄ but larger than GdPO₄. The diminished lattice parameters (compared with CePO₄) indicate that the additional phase is not pure monazite CePO₄, but may be an incorporated phosphate monazite (CeGd)PO₄.

Table 3 shows the point analysis of the additional phase layer indicated in the SEM image of Fig. 6. The point analyses shown in Table 3 were also used as reference due to the detection limitation of EDX measurement. Based on the lattice parameter indicated in Table 2 and the XRD results shown in Fig. 5, the main phase of Spectrum 1, 2 and 3 is (Ce_{0.9}Gd_{0.1})PO₄, and the main phase of Spectrum 4–9 was GDC. The atomic ratio of Gd: Ce in Spectra 1–9 in Table 3 show small deviations from the theoretical value of Ce_{0.9}Gd_{0.1}O₂, which is attributable to the measurement error of EDX device.

4. Discussion

4.1. Reaction mechanism of YSZ

In present case, the $p(O_2)$ of CSG was mainly dominated by H₂/H₂O equilibrium due to the slow equilibrium reaction of CO/CO₂. Ellingham diagram for the P–H–O system has been reported by Kishimoto et al. [24]. At 900 °C, PH₃ was easily oxidized in P₂O₅ in

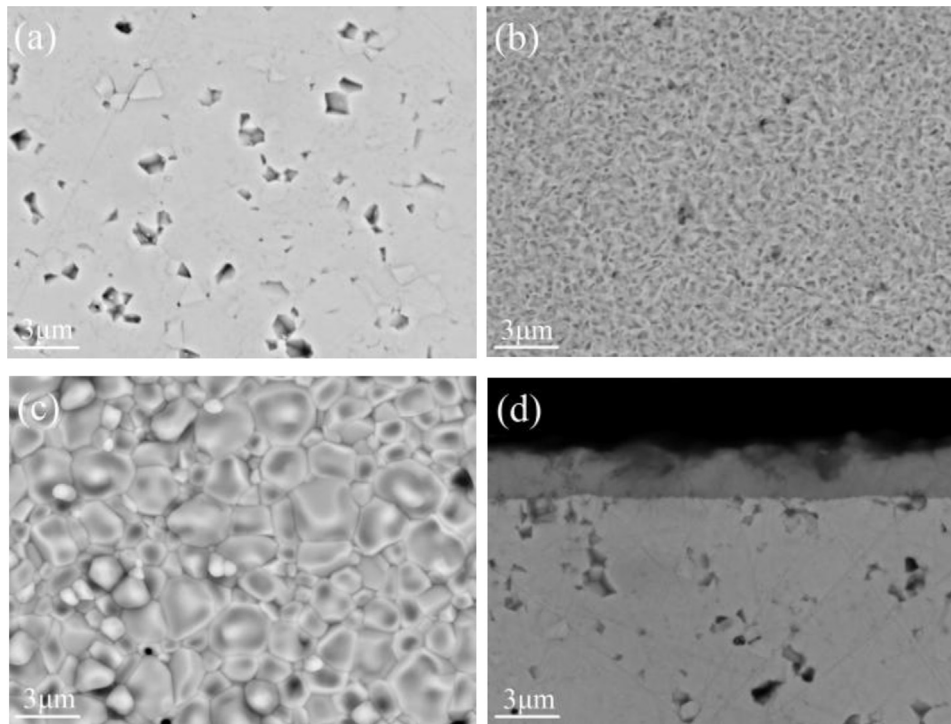
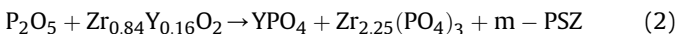
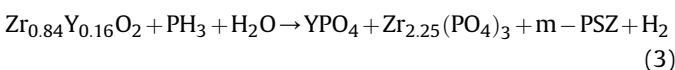


Fig. 4. SEM images of the surface and the cross section of GDC pellets before and after exposure to different conditions, (a) surface of fresh pellet, (b) surface after exposure to CSG1 with 1 ppm PH₃, (c) surface after exposure to CSG1 with 10 ppm PH₃, (d) cross section after exposure to CSG1 with 10 ppm PH₃.

the region with relative high oxygen potential. Aggregate results for YSZ indicate that the main reaction between YSZ and 10 ppm PH₃ can be expressed as:



It also could be writing as following:



The YPO₄ layer generated on the surface of YSZ (as depicted in Fig. 3) indicates that formation depends on diffusion of bulk Y to the YSZ surface. Formation of m-PSZ indicates that the Y reaction with PH₃ is more active, and the stability of YPO₄ is better than that of Zr_{2.25}(PO₄)₃. Phase transformation (from cubic to monoclinic) in YSZ results from decreasing the Y₂O₃ concentration [31–33]. In this case, quantification of the Y concentration in m-PSZ is not possible since it may be very low and transitional. As depicted in Fig. 3 and reported in Table 1, four stratified layers were formed owing to chemical reactions and elemental diffusion. From surface to interior the layers are: YPO₄, Zr_{2.25}(PO₄)₃, m-PSZ plus minor YPO₄, and YSZ layer, respectively. From these, we can deduce that several conditions are required to form the heterophase multi-layers: (1) Y reacts with low concentrations of phosphorus; (2) Zr only reacts with relatively high concentrations of phosphorus; (3) Y could diffuse into m-PSZ and YSZ; (4) Y cannot diffuse into Zr_{2.25}(PO₄)₃.

To better understand how the reactions occurred on YSZ pellet with 10 ppm PH₃ exposure, a possible reaction schematic is depicted in Fig. 7. Three sequential steps are postulated.

In step 1, PH₃ in CSG firstly reacts with Y on the surface of YSZ and forms the YPO₄ due to relatively high reactivity of Y in YSZ. Meanwhile, segregation of Y in YSZ results in formation of m-PSZ in place. In step 2, the Zr in m-PSZ possesses relatively higher chemical potential than in 8 mol% YSZ and reacts with PH₃ and H₂O to form Zr_{2.25}(PO₄)₃. More YPO₄ and m-PSZ form on the surface and interior of YSZ in step 2 owing to bulk diffusion of Y to the pellet surface. Y existing in the m-PSZ layer and in YPO₄ near the m-PSZ layer rapidly reacted or diffused in this step.

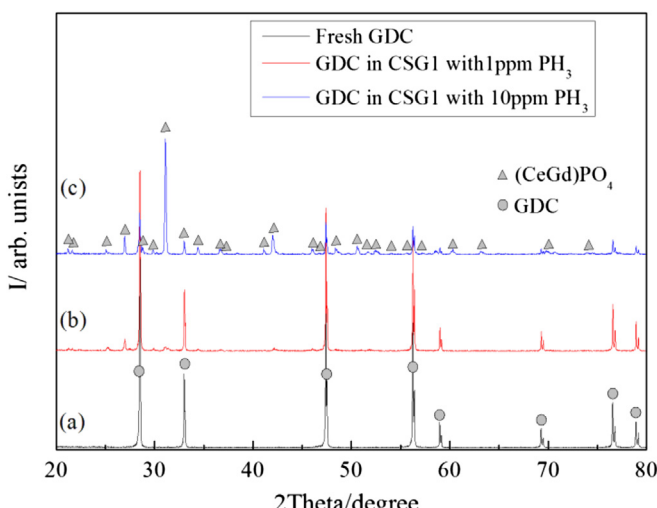
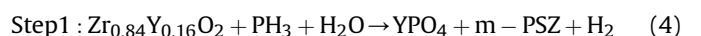


Fig. 5. XRD patterns of the surface of GDC pellets before after exposure to CSG1 with different PH₃ concentrations, (a) fresh pellet, (b) in CSG1 with 1 ppm PH₃, (b) in CSG1 with 10 ppm PH₃.

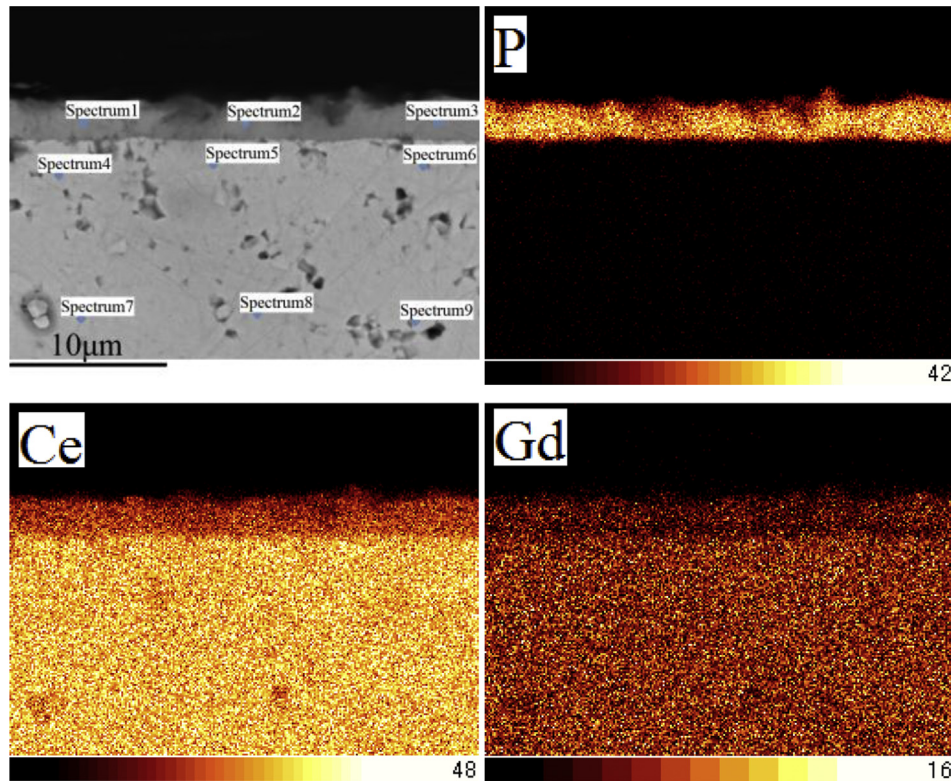


Fig. 6. Elemental maps of the cross section of GDC pellet after exposure testing in CSG1 with 10 ppm PH₃.

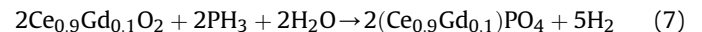
The scattered Zr_{2.25}(PO₄)₃ nucleated and grew with annealing time in step 2, eventually coalescing to form a dense layer in step 3. From point analysis result of Y shown in Table 1 and the Y map shown in Fig. 3, no Y exists in Zr_{2.25}(PO₄)₃ layer, which indicates that Y does not diffuse into the Zr_{2.25}(PO₄)₃ layer. In other words, no more YPO₄ was formed on the surface of YSZ after the dense Zr_{2.25}(PO₄)₃ layer formed under the surface YPO₄ layer. Scattered YPO₄ formed under dense Zr_{2.25}(PO₄)₃ layer shown in Fig. 3 indicates that the activity of P in m-PSZ is sufficient to form YPO₄ (as indicated in Eq. (6)), but insufficient to form Zr_{2.25}(PO₄)₃. Here, to form such scattered YPO₄, Y should diffuse from inside of m-PSZ or YSZ until the chemical potential of P diminishes to the minimum value for Y reaction. In this study, no obvious chemical reactions occurred on the surface of YSZ after exposure to CSG1 with 1 ppm PH₃, indicating that the reactivity of Y and Zr in YSZ may be insufficient to react with 1 ppm PH₃ in CSG1. The zirconia electrolytes are potentially compatible electrolytes for CSG containing 1 ppm level PH₃ in SOFC.

4.2. Reaction mechanism of GDC

Data presented in Fig. 6 and Table 3 for the GDC pellet indicate that a (Ce_{0.9}Gd_{0.1})PO₄ layer formed on the surface after exposure to CSG1 with 10 ppm PH₃. A possible reaction is expressed as:

Table 2
Lattice parameter of additional phase formed on the surface of GDC.

Materials	Lattice parameters						
	<i>a</i> (Å)	<i>b</i> (Å)	<i>c</i> (Å)	α (°)	β (°)	γ (°)	<i>V</i> (Å ³)
(CeGd) PO ₄	6.779	7.014	6.454	90°	103.19°	90°	298.77
CePO ₄ [19]	6.788	7.016	6.465	90°	103.43°	90°	299.92
GdPO ₄ [20]	6.621	6.823	6.31	90°	104.16°	90°	276.6



Clavier et al. summarized that the natural monazites generally can incorporate lanthanides from lanthanum to lutetium with various chemical compositions, and La and Ce are identified as predominant in most cases [30]. The formation of homogeneously incorporated monazites with solid state reaction method requires stringent conditions in temperature, elements, and atmosphere [30,34]. The separation of YPO₄ and Zr_{2.25}(PO₄)₃ in YSZ sample in this study also indicates that the formation of incorporated monazites requires specific conditions. In this case the formation of (Ce_{0.9}Gd_{0.1})PO₄ indicates that Ce and Gd might have similar

Table 3
Point analysis of the additional phase layer indicated in cross section SEM image of Fig. 6.

Spectrum no.	Elemental (at.%)				Possible phase compositions
	O	Ce	Gd	P	
Spectrum 1	63.5	15.8	1.7	19.0	(Ce _{0.9} Gd _{0.1})PO ₄
Spectrum 2	60.4	17.1	2.1	20.4	
Spectrum 3	63.9	15.4	1.8	18.9	
Spectrum 4	66.0	30.5	3.4	0	GDC
Spectrum 5	67.0	30.0	2.9	0.1	
Spectrum 6	66.6	29.8	3.4	0.2	
Spectrum 7	68.1	29.2	2.8	0	
Spectrum 8	67.9	28.7	3.4	0	
Spectrum 9	67.3	29.1	3.5	0	

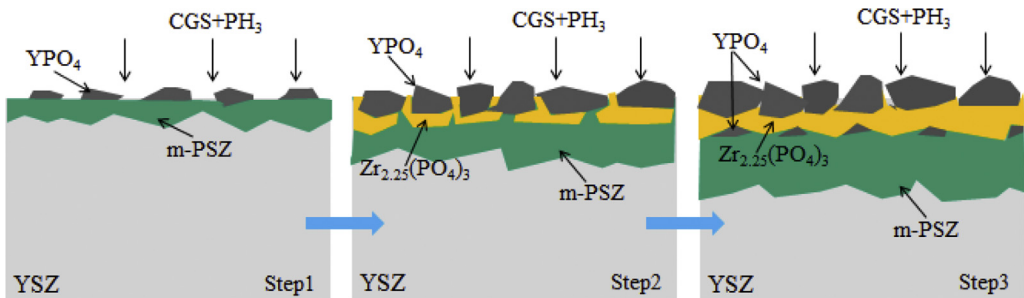


Fig. 7. Postulated reaction schematic between YSZ and 10 ppm PH₃ in CGS.

chemical reaction potentials with PH₃ in the CSG atmosphere, therefore Ce and Gd might react simultaneously with PH₃. Exposure test results of GDC indicate that the reactivity of 1 ppm PH₃ is sufficient for both Ce and Gd. Future use of GDC in a coal syngas fuelled cell requires examination of GDC reactivity with PH₃ at much lower PH₃ concentrations.

5. Conclusions

The chemical potential of 10 ppm PH₃ in coal syngas is sufficient to react with YSZ. YSZ showed good phosphorus resistance at 1 ppm PH₃ exposure in CSG. Segregation and diffusion of yttrium in YSZ are the dominant processes for chemical reactions between YSZ and PH₃ in CGS with 10 ppm PH₃. Stratified YPO₄, Zr_{2.25}(PO₄)₃ and monoclinic Y partial stabilized ZrO₂ formed sequentially from the surface to interior of the YSZ after exposure to CSG2 with 10 ppm PH₃. (Ce_{0.9}Gd_{0.1})PO₄ was formed on the surface of both GDC pellets after exposure to CSG with 1 ppm PH₃ and with 10 ppm PH₃, indicating that GDC is more susceptible to degradation in CSG containing 1 ppm PH₃ than YSZ.

Acknowledgements

This study was supported by Japan-U.S. Collaboration on Clean Energy Technology. The authors thank Prof. Dr. Harumi Yokokawa at National Institute of Advanced Industrial Science and Technology of Japan for his helpful discussions and advice.

References

- [1] M. Li, A.D. Rao, J. Brouwer, G.S. Samuelsen, J. Power Sources 195 (2010) 5707–5718.
- [2] G.Q. Guan, C. Fushima, A. Tsutsumi, M. Ishizuka, S. Matsuda, H. Hatano, Y. Suzuki, Particulology 8 (2010) 602–606.
- [3] Y. Kobayashi, Y. Ando, M. Nishiura, H. Kishizawa, M. Iwata, N. Matake, K. Tomida, ECS Trans. 57 (2013) 53–60.
- [4] R. Nii, Y. Komatsu, S. Kimijima, ECS Trans. 57 (2013) 3049–3058.
- [5] F.N. Cayan, M. Zhi, S.R. Pakalapati, I. Celik, N. Wu, R. Gemmen, J. Power Sources 185 (2008) 595–602.
- [6] N.P. Trembley, R.S. Gemmen, D.J. Bayless, J. Power Sources 163 (2007) 986–996.
- [7] G.A. Hackett, K. Gerdes, X. Song, Y. Chen, V. Shutthanandan, M. Engelhard, Z. Zhu, S. Thevuthasan, R. Gemmen, J. Power Sources 214 (2012) 142–152.
- [8] J.P. Viricelle, P. Breuil, G. Tournier, M. Minot, C. Pijolat, Procedia Eng. 25 (2011) 1089–1092.
- [9] V.V. Plashnitsa, S.A. Anggraini, N. Miura, Electrochim. Commun. 13 (2011) 444–446.
- [10] N.P. Padture, M. Gell, E.H. Jordan, Science 296 (2002) 280–284.
- [11] M. Zhao, W. Pan, Acta Mater. 61 (2013) 5496–5503.
- [12] W.F. Jeffrey, J. Power Sources 162 (2006) 30–40.
- [13] H. Yokokawa, N. Sakai, T. Horita, K. Yamaji, M.E. Brito, MRS Bull. 30 (2005) 591–595.
- [14] J. Bao, G.N. Krishnan, P. Jayaweera, J. Perez-Mariano, A. Sanjurjo, J. Power Sources 193 (2009) 607–616.
- [15] M. Zhi, X. Chen, H. Finklea, I. Celik, N.Q. Wu, J. Power Sources 183 (2008) 485–490.
- [16] C. Xu, J.W. Zondlo, M. Gong, X.B. Liu, J. Power Sources 196 (2011) 116–125.
- [17] K.C.R. De Silva, B.J. Kaseman, D.J. Bayless, Int. J. Hydrogen Energy 36 (2011) 9945–9955.
- [18] K. Haga, Y. Shiratori, Y. Nojiri, K. Ito, K. Sasaki, J. Electrochim. Soc. 157 (11) (2010) B1693–B1700.
- [19] O.A. Marina, C.A. Coyle, E.C. Thomsen, D.J. Edwards, G.W. Coffey, L.R. Pederson, Solid State Ionics 181 (2010) 430–440.
- [20] J.F.B. Rasmussen, A. Hagen, J. Power Sources 191 (2009) 534–541.
- [21] L. Zhang, S.P. Jiang, H.Q. He, X. Chen, J. Ma, X.C. Song, Int. J. Hydrogen Energy 35 (2010) 12359–12368.
- [22] M. Cooper, K. Channa, R. De Silva, D.J. Bayless, J. Electrochim. Soc. 157 (11) (2010) B1713–B1718.
- [23] O. Demircana, W. Zhang, C. Xu, J. Zondlo, H.O. Finkle, J. Power Sources 195 (2010) 3091–3096.
- [24] H. Kishimoto, K. Yamaji, M.E. Brito, T. Horita, H. Yokokawa, J. Min. Metall. B Metall. 44 (2008) 39–48.
- [25] P. Gansor, C. Xu, K. Sabolsky, J.W. Zondlo, E.M. Sabolsky, J. Power Sources 198 (2012) 7–13.
- [26] M. Gong, D. Bierschenk, J. Haag, K.R. Poeppelmeier, S.A. Barnett, C. Xu, J.W. Zondlo, X. Liu, J. Power Sources 195 (2010) 4013–4021.
- [27] G. Chen, H. Kishimoto, K. Yamaji, K. Kuramoto, M.Y. Gong, X.B. Liu, G. Hackett, K. Gerdes, T. Horita, ECS Trans. 57 (2013) 1577–1583.
- [28] Y. Ni, J.M. Hughes, A.N. Mariano, Am. Mineral. 80 (1995) 21–26.
- [29] D.F. Mullica, A.A. Grossie, L.A. Boatner, Inorg. Chim. Acta 109 (1985) 105–110.
- [30] N. Clavier, R. Podor, N. Dacheux, J. Eur. Ceram. Soc. 31 (2011) 941–976.
- [31] R.H.J. Hannink, J. Am. Ceram. Soc. 83 (2000) 461–487.
- [32] Y.Y. Chen, W.C.J. Wei, Solid State Ionics 177 (2006) 351–357.
- [33] R. Ramamoorthy, D. Sundararaman, S. Ramasamy, Solid State Ionics 123 (1999) 271–278.
- [34] D. Bregiroux, O. Terra, F. Audubert, N. Dacheux, V. Serin, R. Podor, D. Bernache-Assollant, Inorg. Chem. 46 (2007) 10372–10382.